VII International Conference on Textile Composites and Inflatable Structures
STRUCTURAL MEMBRANES 2015
E. Oñate, K.-U.Bletzinger and B. Kröplin (Eds)

TORSION/BENDING ELEMENTS FOR DR MODELLING OF TUBULAR BEARING STRUCTUES

STRUCTURAL MEMBRANES 2015

SIGRID ADRIAENSSENS[*] AND MICHAEL BARNES[†]

[*] Department of Civil and Environmental Engineering
Princeton University
Olden Street, Princeton, NJ 08544, USA
E-mail: sadriaen@princeton.edu – Web page : http://formfindinglab.princeton.edu/

[†] Department of Architecture and Civil Engineering
University of Bath, UK

Key words: Torsion/Bending, elastic rod, form finding, dynamic relaxation

Summary: The paper presents a three degree of freedom formulation for the dynamic relaxation modelling of tubular bearing systems applied in arch supported membranes and closed hoop supported cable net bridging structures. For tubular arch structures the numerical modelling method has been validated against analytical and finite element models with span/rise ratios up to 20. Beyond this, and particularly as arches flatten under limit state loads the method becomes impractical. A revised process is given for the modelling when approaching failure states, and is applied and validated for the case of a very flexible arch supported membrane structure subject to snap through buckling. The paper also illustrates how the torsion/bending theory can be used to cover different closed hoop supporting systems, and the numerical modelling is applied to a multi-span bridging structure employing tubular hoops of various sizes and shapes around which spiral a prestressed cable network.

1 DYNAMIC RELAXATION

The description of Dynamic Relaxation (DR) summarized briefly below for skeletal and membrane structures assumes kinetic damping to obtain a static equilibrium state. In this procedure the undamped motion of the structure is traced and when a local peak in the total kinetic energy of the system is detected, all velocity components are set to zero. The process is then restarted from the current geometry and repeated through further generally decreasing peaks until the energy of all modes of vibration has been dissipated and static equilibrium is achieved. The initial concept for dynamic relaxation can be expressed as Newton's second law governing the motion of any node i in direction *x* at time *t*. Writing the acceleration term in finite difference form and rearranging the equation gives a recurrence equation for updating velocity components:

$$v_{ix}^{t+\Delta t/2} = \frac{\Delta t}{M_i} R_{ix}^{t} + v_{ix}^{t-\Delta t/2} \qquad \textit{(at all nodes i in directions x,y,z)} \tag{1a}$$

Hence obtain the updated geometry projected to time $t+\Delta t/2$; having obtained the complete current geometry the new link forces can be determined and resolved together with applied load components Pix to give the updated residuals:

$$R_{ix}^{t+\Delta t} = P_{ix} + \sum (\frac{F}{L})_m^{t+\Delta t} (x_j - x_i)^{t+\Delta t} \quad \textit{(for all links m at node i)} \tag{1b}$$

The procedure is thus time stepped using Eqs.1a & 1b until a kinetic energy peak is detected. Velocity components are then reset to zero and the process is repeated until adequate convergence with negligible kinetic energy is achieved. In equation 1b the term $(F/L)_m$ is the current tension coefficient in any link *m* - a cable, strut or side of a membrane element [1].

2 IN-PLANE BENDING

Figure 1a represents consecutive nodes along an initially straight tubular (CHS) beam traverse, and figure 1b two adjacent deformed segments, a & b, viewed normal to the plane of nodes ijk which are assumed to lie on a circular arc of radius R. The spacing of nodes along the traverse must be sufficiently close to allow this assumption, but the segment lengths need not be equal.

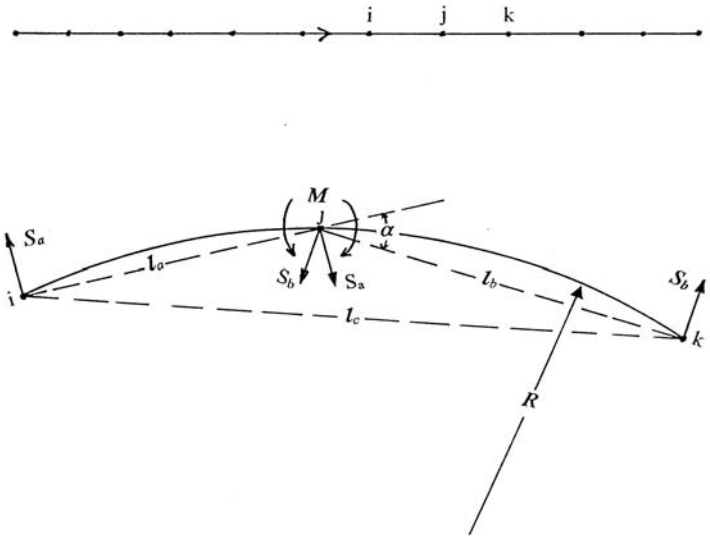

Figure 1a & 1b

From the geometry of the figure the angle subtended by the chord l_c at the centre of radius R is 2α, and thus the radius of curvature through i j k and the consequent moment in the arc are:

$\boldsymbol{R} = \dfrac{\boldsymbol{l_c}}{\boldsymbol{2\sin\alpha}}$ and $\boldsymbol{M} = \dfrac{\boldsymbol{EI}}{\boldsymbol{R}}$ where ***EI*** is assumed constant along the traverse.

The free body shears of elements a and b complying with moment M at j are therefore:

$$\boldsymbol{S_a} = \frac{\boldsymbol{2EI \cdot \sin\alpha}}{\boldsymbol{l_a \cdot l_c}} \quad ; \quad \boldsymbol{S_b} = \frac{\boldsymbol{2EI \cdot \sin\alpha}}{\boldsymbol{l_b \cdot l_c}} \tag{2}$$

These must be taken as acting normal to the chords and in the local plane of i j k. The calculations and transformations required in a DR scheme are thus very simple, with sets of three consecutive nodes being considered sequentially along the entire traverse; each set lying in different planes when modelling a spatial curve.

2.1 Out of plane bending of a closed ring

It might be questioned whether the above is applicable to a spatially twisted spline since apparently no torsional stiffness enters into the analysis; yet in fact this is the case provided the spline is initially straight and with ***EI*** constant about any axis. Taking a simple example of an initially straight tube bent into a closed ring of radius ***R***, with equal and opposite loads ***P*** applied at the quarter points normal to the plane of the ring (figure 2):

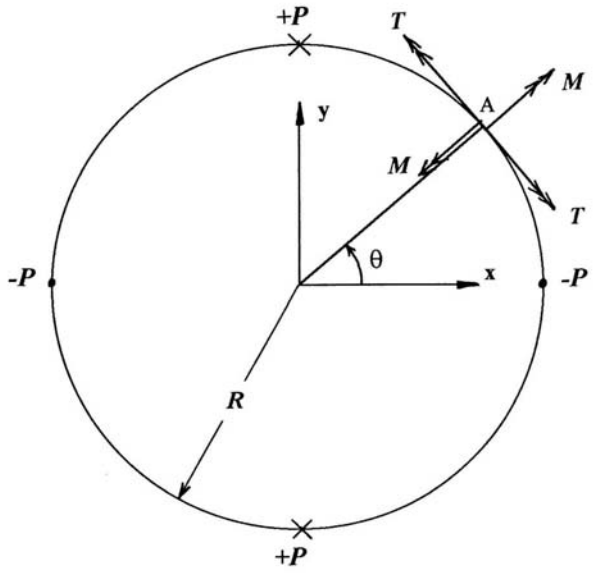

Figure 2

If the bending moment about a radial axis at A is $\boldsymbol{M}$ and the torsion at this location is $\boldsymbol{T}$, then moment equilibrium about axes parallel to x and y through A give:

$$\frac{\boldsymbol{PR}}{\mathbf{2}}\left(\mathbf{1}-\mathbf{sin}\,\boldsymbol{\theta}\right)=\boldsymbol{M}\,\mathbf{cos}\,\boldsymbol{\theta}+\boldsymbol{T}\,\mathbf{sin}\,\boldsymbol{\theta}\quad;\quad\text{and}\quad\frac{PR}{2}\left(1-\cos\theta\right)=T\cos\theta-M\sin\theta$$

$$\text{thus:}\quad\boldsymbol{T}=\frac{\boldsymbol{PR}}{\mathbf{2}}\left(\mathbf{sin}\,\boldsymbol{\theta}+\mathbf{cos}\,\boldsymbol{\theta}-\mathbf{1}\right)\quad;\quad\boldsymbol{M}=\frac{\boldsymbol{PR}}{\mathbf{2}}\left(\mathbf{cos}\,\boldsymbol{\theta}-\mathbf{sin}\,\boldsymbol{\theta}\right)\quad;\quad\text{and}\quad\boldsymbol{M}=\frac{\boldsymbol{dT}}{\boldsymbol{d\theta}}\tag{3}$$

But the prestressing moment (about an axis normal to the plane of the ring) is $\boldsymbol{EI}/\boldsymbol{R}$, and the component of this along the axis of $\boldsymbol{T}$ is:

$$\boldsymbol{T}^{\backslash}=\frac{\boldsymbol{EI}}{\boldsymbol{R}}\cdot\frac{\boldsymbol{dw}}{\boldsymbol{Rd\theta}}\tag{4}$$

Where $\boldsymbol{w}$ is the normal displacement. Differentiating this gives the full elastic stiffness moment:

$$\boldsymbol{M}=\boldsymbol{EI}\frac{\boldsymbol{d^2w}}{\boldsymbol{R^2d\theta^2}}\tag{5}$$

Thus the whole of torsion $\boldsymbol{T}$ is due to the prestressing effect (of bending the initially straight spline tube into a closed ring), and there is no component due to twisting and elastic torsion constant $\boldsymbol{GJ}$.

Substituting $\boldsymbol{T}$ or $\boldsymbol{M}$ from equations (3) into (4) or (5), and integrating gives:

$$\boldsymbol{w}=\frac{\boldsymbol{PR^3}}{\boldsymbol{2EI}}\left(-\mathbf{cos}\,\boldsymbol{\theta}+\mathbf{sin}\,\boldsymbol{\theta}-\boldsymbol{\theta}\right)\;+\;\text{constant}$$

If $\boldsymbol{\Delta}$ is the displacement of the downward loads relative to the upward loads then:

$$\boldsymbol{\Delta}=\frac{\boldsymbol{PR^3}}{\boldsymbol{EI}}\left(\mathbf{1}-\frac{\boldsymbol{\pi}}{\mathbf{4}}\right)\tag{6a}$$

For the same ring, but unstrained in its initial circular state, the displacement(s) corresponding to the same out-of-plane loading can be shown to be:

$$\boldsymbol{\Delta}=\frac{\boldsymbol{PR^3}}{\boldsymbol{2EI}}\left(\frac{\boldsymbol{\pi}}{\mathbf{2}}-\mathbf{1}\right)+\frac{\boldsymbol{PR^3}}{\boldsymbol{2GJ}}\left(\boldsymbol{\pi}-\mathbf{3}\right)=\boldsymbol{\delta}_{\mathbf{m}}+\boldsymbol{\delta}_{\mathbf{t}}\tag{6b}$$

where $\boldsymbol{\delta}_{\mathbf{m}}$ is the component due to transverse bending and $\boldsymbol{\delta}_{\mathbf{t}}$ is the component due to torsion.

It is interesting to note that the out-of-plane stiffness given by Eqn. (6a) which is due principally to geometric stiffening by initial straining, is greater than that given by Eqn. (6b). (in contrast, the in-plane stiffness is identical for both provided EI is the same).

2.2 Extension to approximate analysis of circular arches

For membrane structures supported by pin-ended circular arches of radius $\boldsymbol{R_0}$ which are initially unstrained at this radius, equations 2 with a 3 degree of freedom analysis can still be used provided "initial state" shears $\boldsymbol{S}_1$ and $\boldsymbol{S}_2$ are applied to the two end segments throughout the analysis, as shown in figure 3. Provided both sets of shears are applied in the common plane defined by the two end vectors $\boldsymbol{l_1}$ and $\boldsymbol{l_2}$, the shears must balance statically for the structure as a whole no matter what may be the spatial deformations.

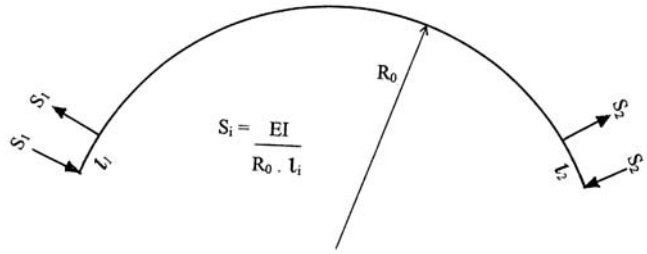

Figure 3

Note that if these shears were applied to the end segments of an originally straight spline, all nodes along the spline would lie exactly on an arc of radius $\boldsymbol{R_0}$ (irrespective of any variations in segment lengths); the shears are required in the analysis to give the initial arc state, and although it is clearly highly strained in this state, all of the interior shears cancel – so the effect is the same as an unstrained arc. When calculating in-plane moments at the end of an analysis the effect of $\boldsymbol{R_0}$ must obviously be accounted for using $\boldsymbol{M = EI\left(1/R - 1/R_0\right)}$, where $\boldsymbol{R}$ is the local radius of the deformed arc. Out-of-plane moments could be determined using displacements normal to the average plane of the deformed arc, but these would be inaccurate since they are derived from incorrect (over stiff) transverse deformations. As stated above, for membranes which are mechanically fixed to an arch the analysis is approximate since the value of $\boldsymbol{EI}$ would correspond to the stiffness in only one direction – the radial direction for in-plane bending of the arch; and the out-of-plane stiffness is not correct. However, for the case of membranes supported over circular arc hoops this is of no consequence since slight slip of the membrane over the arch will anyway occur. A similar argument justifies the use of this approach for "battened" membranes.

3 ACCOUNTING FOR TORSION & TRANSVERSE BENDING IN INITIALLY UNSTRAINGED SPATIAL TRAVERSES

The limitations of the above analysis are more severe when it comes to the analysis of compound traverses consisting of a sequence of circular arcs with different radii. Although each segment might be analysed as above by the use of fictitious end shears (as in figure 3), there would be no torsional connection between the segments, so a compound arch modelled in such a way would become a mechanism. The following theory accounts for torsion and transverse bending moments in compound tubular traverses, in addition to the modelling of the radial moments as previously described. In most practical design cases, both deformations (transverse and radial deflections) and moments (torsional, transverse and radial bending) may be correctly modelled. This is achieved by applying an artificial "torsional factor" (which is the factor by which the real torsional stiffness **GJ** must be reduced in order that transverse deformations (ie normal to the arch plane) may be correctly modelled. In some other more restrictive cases, for example with arch systems with a very low rise to span ratio (eg < 1/40) and/or slenderness ratios which are very high (eg > 500), the transverse deformations will be incorrectly modelled since the arch will be too stiff in the transverse direction (see sections 3.5. and 3.6).

With only three degrees of freedom (u, v, w) it is possible to determine by finite difference modelling the in-plane distortions and moments (fig 1b) and the increment of twist and hence torsion in each link element of a spatially curved traverse (see following section); but it is not possible to determine directly also the transverse bending deformations. However, assuming that the lines of action of all forces exerted by connecting elements such as cables or membranes act through the centerline of the tubular traverse (ie with no applied torsion forces), then the transverse moments are always statically related to the rate of change of torsions in the traverse. Considering a small element of the traverse viewed normal to its local plane:

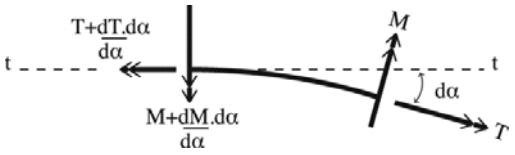

Figure 4

Resolving for equilibrium of moments along axis t – t:

$$T+dT.d\alpha = M.\sin(d\alpha) + T.\cos(d\alpha) \sim> M.d\alpha + T \text{ for } \alpha \sim> 0 \quad (7)$$

$d\alpha$

Hence:

$$M = \frac{dT}{d\alpha} \quad (8)$$

Thus if the torsion in consecutive elements and the local (in-plane) curvature is known the transverse (out-of-plane) moment at the interconnecting node can be determined from eqn. 8.

The in-plane moment (fig 1b) was determined using two consecutive links. The amount of twist in any link and hence the torsion must be determined by considering three consecutive links (fig 5a):

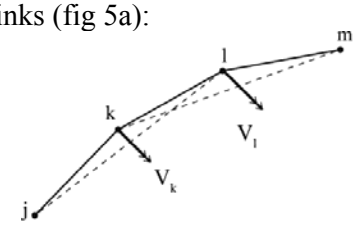

Figure 5a

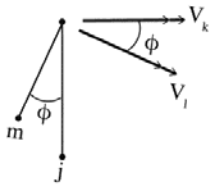

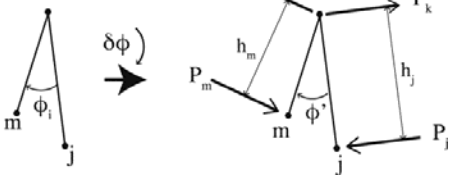

Figure 5b

V_k & V_l are the normal direction cosine vectors of triangles jkl and klm which determine the current twist angle between them φ', or the initial unstressed state of twist φ_i .

Suppose change due to deformation is as shown in figure 5b, where $\varphi' > \varphi_i$:
Restoring forces at m and j due to torsion in kl are as shown: $\mathbf{P_m}$ & $\mathbf{P_j}$; and associated forces to restore lateral moment equilibrium must act as shown at k & l: $\mathbf{P_k}$ & $\mathbf{P_l}$.

$\mathbf{P_j}$ and $\mathbf{P_m}$ are related to the Torsion **T** in kl :

$$\mathbf{P_j \,.\, h_j = P_m \,.\, h_m = T = \frac{GJ}{L_{kl}} . (\varphi' - \varphi i)} \tag{9}$$

Where $\mathbf{h_j}$ & $\mathbf{h_m}$ = heights of triangles jkl & klm from base kl.

Considering the static equilibrium of the 3 link unit:

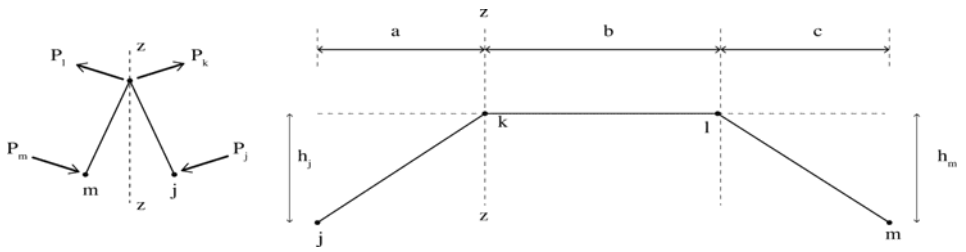

Figure 6

Resolving normal to plane containing axis zz and kl:

$$\mathbf{P_m} \cos(\varphi'/2) + \mathbf{P_k} \cos(\varphi'/2) = \mathbf{P_l} \cos(\varphi'/2) + \mathbf{P_j} \cos(\varphi'/2) \tag{10}$$
$$\mathbf{P_m + P_k = P_l + P_j}$$

Moments about zz (cancelling cos(φ'/2) from each term) give:

$$\mathbf{P_j} \,.\, a + \mathbf{P_m} \,.\, (b + c) = \mathbf{P_l} \,.\, b \tag{11}$$

Hence $\mathbf{P_j}$ & $\mathbf{P_m}$ are determined from (9), and from (11) & (10):

$$\mathbf{P_l} = (\mathbf{P_j} \,.\, a + \mathbf{P_m}.(b + c)) / b \quad \text{and} \quad \mathbf{P_k} = \mathbf{P_l} + \mathbf{P_j} - \mathbf{P_m} \tag{12}$$

Note that in shallow arcs (Assuming similar consecutive element lengths) the forces $\mathbf{P_k}$ & $\mathbf{P_l}$ are typically 3 x teh values of $\mathbf{P_j}$ and $\mathbf{P_m}$, yet it is the latter that are determined directly in the DR process process from current deformations. But the bending forces exerted by successive sets of 3 elements along a traverse will tend to oppose and cancel each other, and will do so exactly if the torsions are constant (eq. 8).

An obvious special case occurs when two consecutive links are or become co-linear so that φ for kl becomes zero. This can occur during snap-through buckling, and this is the major aspect which will be considered in sections 4 and 5 of this paper.

3.1 Torsion Factor for closed ring traverses

During the DR analysis the value of **GJ** (eq 9) will govern the torsional deformations and hence also the associated transverse bending. In the case of the initially unstrained closed ring (figure 2) with four point loading the transverse flexibility for coupled bending and torsion is given by equation 6b, in which **EI** is the value relating to transverse bending (normal to the ring plane). The finite difference (DR) analysis outlined above utilizes only the torsional stiffness to obtain torsional forces from the change in twist angle; the transverse moments being obtained as derivatives of the torsion from equation (8). Thus in the closed ring case shown in figure 2, to obtain deformations which are the same as the real case (as in eq 6b) the torsion constant must be set to $\mathbf{GJ' = T_{fac} .GJ}$, where the "torsional factor" is:

$$\mathbf{T_{fac}} = \boldsymbol{\delta_t} /(\boldsymbol{\delta_m} + \boldsymbol{\delta_t}) \qquad \mathbf{T_{fac}} = 1 / (1 + 4.03\, C_1) \;\text{ with } C_1 = \mathbf{GJ/EI_t} \tag{13}$$

For a CHS steel tube the EI_t value for transverse bending is identical to that for in-plane bending and if the value of $C_1 = 0.8$ then $T_{fac} = 0.237$ (or with $C_1 = 1$ then $T_{fac} = 0.199$, but note that the difference in deflections given by equation 6b would be only approximately 4%).

Numerical tests analyzing closed ring structures with a range of different diameters and tubular section sizes have shown that deformations, torsions, in-plane moments and out-of-plane moments are all accurately predicted using the above theory.

3.2 Extension to oval hoops with double and single symmetry

The type of analysis applied in section 2.1 for a closed ring under four point transverse loading to derive deformations in the form : $\Delta = \boldsymbol{\delta_m} + \boldsymbol{\delta_t}$ (with $\boldsymbol{\delta_m}$ due to transverse bending and $\boldsymbol{\delta_t}$ due to torsion) can also be applied to doubly symmetric oval shaped hoops defined by radii R and r.

In this case, and simplifying by setting GJ = EI , both $\boldsymbol{\delta m}$ and $\boldsymbol{\delta_t}$ take the form:

$\boldsymbol{\delta} = (a.R^3 + b.R^2.r + c.R.r^2 + d.r^3).P/2EI$

where the coefficients a,b,c,d depend on the ratio r/R and are different for the bending and torsion components of deflection. The torsion factor for use in numerical analyses can then be obtained as $\mathbf{T_{fac} = \delta_t /(\delta_m + \delta_t)}$. For the case of singly symmetric or egg shaped hoops (fig. 7) by suitable adjustment of the ratios r/R in each half the same torsion factor can be applied throughout the hoop.

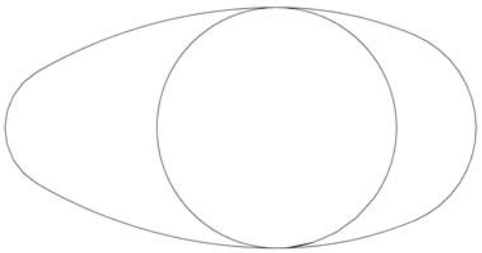

Figure 7

The above type of analysis was applied in reference 2 to a multi-span bridging structure employing tubular hoops of various sizes and shapes around which spiral a prestressed cable network – see figures 8. The top and bottom booms are connected to the hoops by internal diagonal bracings and the booms are connected to each-other only by vertical ties; the bridge deck would correspond with the level of the lower boom. The scale of the bridge, with enclosed spans of typically 100m and deck width of 6.5m, is suitable for pedestrians, cyclists and small electric vehicles, and the structure was assessed for appropriate design load states and resilience to collapse.

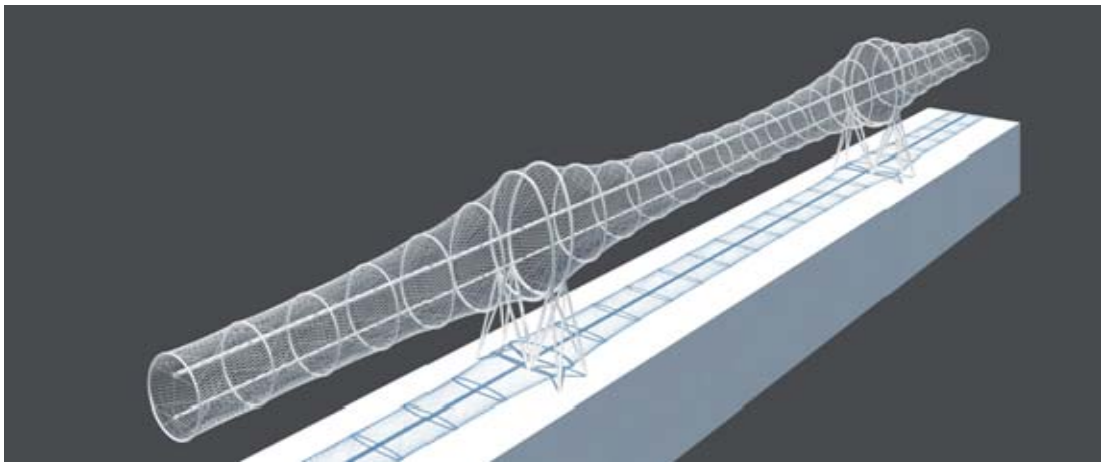

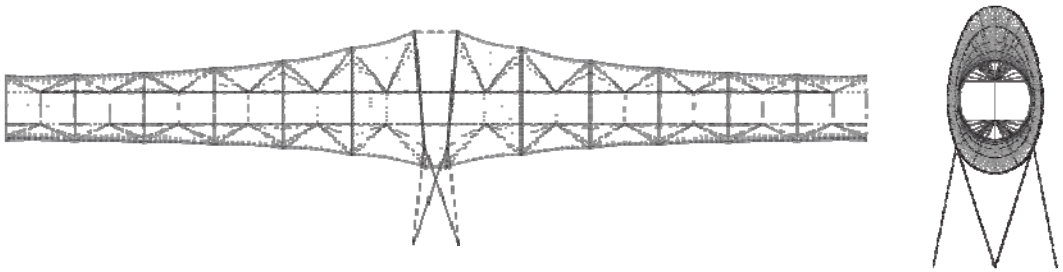

Figure 8: Perspective and elevations of one multi-span section

3.3 Torsion factor for open arches

In general, for open arch traverses, the torsion factor may vary quite widely depending particularly on the radius of curvature of the arch and the total arc length, but also being limited by the slenderness ratio and the rise / span ratio. Values for torsion factor in the case of open arches might be assessed by considering a circular arc beam with equal and opposite loads P applied transverse to the arch at the ¼ points, as shown in figure 9:

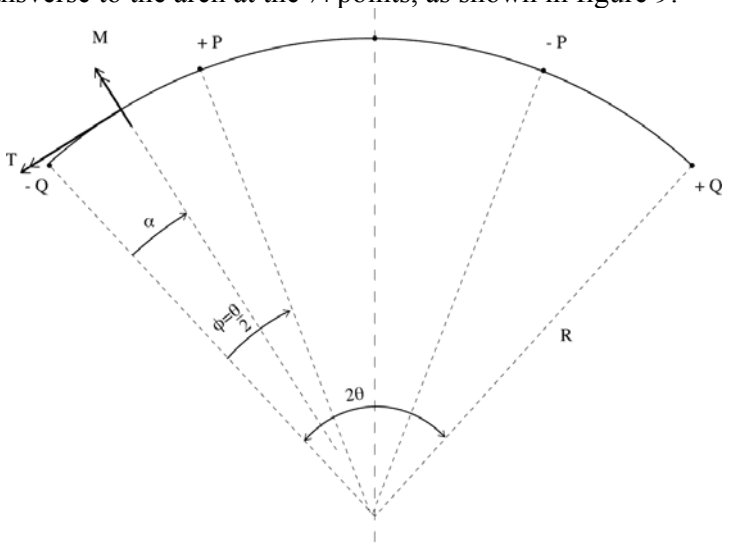

Figure 9

The end reactions $Q = P(\sec\varphi)/2$, where $\varphi = \theta/2$

For $0 < \alpha < \varphi$: the transverse moment $M = Q.R.\sin\alpha$ & torsion $T = Q.R(1 - \cos\alpha)$
For $\varphi < \alpha < \theta$: $M = Q.R.\sin\alpha - P.R.\sin(\alpha - \varphi)$ &
$T = P.R(\cos(\alpha - \varphi) - 1 + \sec\varphi.(1-\cos\alpha)/2)$

The deflection of the ends (at Q) relative to the ¼ point positions (at P) can be derived as two components; the first associated with transverse bending alone is:

$$\delta_m = K \,.\, P.R^3 / 2EI_t \tag{14a}$$

Where:

$$K = (\varphi.\sec\varphi - \sin\varphi)/2 \tag{14b}$$

The second component due solely to torsion can be derived as:

$$\delta_t = k \,.\, PR^3 / 2GJ \tag{15a}$$

Where:

$$k = \varphi\,(2.5\sec\varphi + 2\cos\varphi - 3) - \sin\varphi\,(\sec\varphi + 0.5) \tag{15b}$$

In the DR analysis, the total transverse deformations are based only on the twists and torsions related to a reduced torsion constant, T_{fac} x GJ, the torsion factor must therefore be set equal to:

$$T_{fac} = \delta_t / (\delta_t + \delta_m) = k / (k + C_1 K) \text{ , where as before } C_1 = GJ / EI_t \tag{16}$$

All of the above relates to the particular test case of transverse loadings at the ¼ points of arch beams (with end reaction loads also normal to the arch), and the values of T_{fac} predicted, although independent of loading magnitude, may not be independent of loading distributions; however it does enable approximate modelling of the transverse flexibility so that the interactions between membrane surface fields and a supporting arch can be accounted for.

3.4 Numerical Stability & Convergence

Numerical stability of the DR process is controlled by fictitious mass components used at each node. These mass components are directly proportional to the stiffness of elements attached to a node. The elastic axial stiffness of an element is **EA/L**, and the bending stiffness of an arch beam element is $\mathbf{2EI/L^3}$. However, it can be shown that the stiffness of a node due to the coupled torsional & transverse bending effect is $\mathbf{K \,.\, (EI/L^3).\, (R/L)^2}$, where R is the in-plane radius of curvature and L is the element length. The value of K ~> 1, and thus since generally R >>L, the coupled torsion / bending stiffness and its contribution to the nodal mass components will be much greater than for ordinary elastic bending (eg the in-plane bending). As a consequence of these increased mass components the convergence rate is slower for this type of analysis. All of the nodal mass components are set automatically within the numerical process, thus the problem of numerical divergence is not an issue. However, a type of quasi-stability can occur when the bending stiffnesses (in-plane or coupled torsion / bending) are greater than the axial stiffness – and that may occur when element lengths are very small.

3.5 Numerical test cases

The following series of tests are for CHS circular arches of 100m span and varying radii of curvature such that the ratios of (0.5 x arc length/radius of curvature) comply with the practical range $\pi/4 - \pi/16$ (or rise/span ratios of 5 – 20). For each test case a comparison is made with the theoretical predictions for:

deflection at the ¼ point : $\Delta = \delta_m + \delta_t$ from equations 14 & 15,
transverse moment at the ¼ point $M_q = 0.5P.R.\tan(\theta/2)$,
and torsion at the crown $T_c = P.R.(\mathrm{Sin}(\theta/2) - 1)$.

In the numerical tests the arches are all subdivided into 32 elements and values are tabulated for Δ, M_o (the out-of-plane moment corresponding to M_q), M_i (the in-plane moment at the same ¼ point), and the center point torsion T (corresponding to T_c).

These results are each listed for the value of T_{fac} predicted in table 1, with a second value giving a best fit to the theoretical deflection. Non-linear finite element modelling results taken from reference 2 are also given for comparison.

Table 1: Test cases for a series of CHS arches

	θ	**R (radius of curv.)**	**P (loads)**	**δm**	**δ_t**
arc2a	π/4	70.71 m	100kN	0.468	0.127
Theory:		Δ=0.595	MO =1464 kNm		Tc =582 kNm
	Tfac	**Δ**	**MO**	**Mi**	**T**
Numerical:	**0.214**	0.53	1455	118 & -161	581
	0.191	0.594	1452	132 & -181	580
FE model:		0.595	1461	135 & -192	582
	θ	**R (radius of curv.)**	**P (loads)**	**δm**	**δ_t**
arc3a	π/8	130.66 m	100kN	0.355	0.024
Theory:		Δ=0.379	MO =1299 kNm		Tc =256 kNm
	Tfac	**Δ**	**MO**	**Mi**	**T**
Numerical:	**0.064**	0.323	1282	185 & -138	256
	0.055	0.378	1275	219 & -156	256
FE model:		0.381	1298	215 & -153	256
	θ	**R (radius of curv.)**	**P (loads)**	**δm**	**δ_t**
arc4a	π/12	193.19 m	100kN	0.338	0.01
Theory:		Δ=0.348	MO =1272 kNm		Tc =167 kNm
	Tfac	**Δ**	**MO**	**Mi**	**T**
Numerical:	**0.029**	0.3	1248	185 & -310	166
	0.025	0.344	1240	212 & -358	165
FE model:		0.349	1270	210 & -352	167
	θ	**R (radius of curv.)**	**P (loads)**	**δm**	**δ_t**
arc5a	π/16	256.29 m	100kN	0.337	0.005
Theory:		Δ=0.342	MO =1262 kNm		Tc =124 kNm
	Tfac	**Δ**	**MO**	**Mi**	**T**
Numerical:	**0.016**	0.295	1222	240 & -430	123
	0.014	0.346	1207	281 & -516	122
FE model:		0.342	1261	275 & -511	124

For shallower arches it is not possible to obtain the correct lateral deformations because the least value of T_{fac} to obtain convergence is restricted (for example to the value 0.008 in the case below, with span/rise ratio of 40):

Table 2: Test cases for a shallow CHS arch

	θ	R (radius of curv.)	P (loads)	δm	δ_t
arc6a	π/32	510.12 m	100kN	0.329	0.001
Theory:		Δ=0.330	M_O =1253 kNm		T_c =62 kNm
	T_{fac}	**Δ**	**M_O**	**M_i**	**T**
Numerical:	**0.0042**	-	-	-	-
	*0.008	0.155	1211	244 & -620	61

3.6 Discussion of results

The out-of-plane (or transverse) static moments and torsions are in all test cases of acceptable accuracy but the transverse deflection / flexibility, which in the case of coupled arch and membrane structures will also govern the moments and torsions, is predicted with acceptable accuracy only up to a span/rise ratio of 20 (for slenderness ratio of 350). These limits would encompass many practical design cases for service loading conditions, but the apparent restriction on radii of curvature must cause difficulties when attempting ultimate load analyses of slender arches approaching snap-through buckling. As shown in the above tests, the shallower an arch becomes the smaller is the required value of T_{fac} to give the correct flexibility, but there is a limit to T_{fac} below which numerical convergence cannot be obtained. An additional problem in this context is that the effective coupled torsion/ transverse bending stiffness is proportional to $(R/L)^2$ where L is the local element modelling length; the increasing value of R will thus govern the fictitious mass components which must be used in the DR process to ensure stability and convergence. So as snap through buckling is approached the mass factors will need to be greatly increased and simultaneously the value of T_{fac} reduced (with the limit restricted to a least feasible value). The value of T_{fac} governs the transverse deformations and consequently also the amount of stretch and flattening of the arch crown; this in turn governs the in-plane moments that are induced (+ve at the ¼ points and – ve at the crown). These in-plane moments are also related to the amount of twist in the arch, which is greatly increased by the reduced torsion constant (T_{fac} x GJ). But in this context the greatest twist t the quarter points in any of the test cases is approximately 10^o, so it appears that the arch stretching (and associated crown flattening) is the dominant effect. This cannot be predicted by the analytical model; however it is confirmed by the non-linear finite element modelling.

4 ALTERNATIVE MODELLIG USING FICTITIOUS END SHEARS

An important aspect in the design of lightweight and flexible arch supported structures is the assessment of ultimate load states – in particular snap-through buckling; but as noted above, there is a potential problem of modelling snap-through buckling for coupled membrane/arch systems using the torsion / bending analysis approach, especially for very

slender and flexible arches. This is investigated in detail in the next section of this paper, where it is shown that the alternative technique of analyzing an initially unstrained circular arch as a straight spline with end shears superimposed to induce the same initial curvature (figure 3) can provide a more useful approach to the modelling of such failure modes. However, it is instructive first to compare results for a slender bare arch (having properties identical to those used in the next section (5) and slenderness ratio of 530) with those obtained from models using fictitious end shears. The table below compares results for theory and the best deflection fit of the torsion/bending model, and also non-linear Finite Element modelling, with results for the end shears model:

Table 3: Comparison Models

		Analytical		Torsion/Bending		Finite Element		End Shears	
θ	**P**	**δ**	**Mo**	**δ**	**Mo**	**δ**	**Mo**	**δ**	**Mo**
π/2	5	0.603	125	0.602	125			0.166	60
π/4	50	1.082	732	1.078	713	1.081	732	0.763	616
π/8	50	0.69	650	0.695	611	0.7	648	0.635	609
π/16	50	0.622	631	0.336	599	0.612	634	0.606	578
π/32	50	0.6	626	0.085	620			0.599	498 (596)

The End Shears model gives good values for deflections of the shallowest arch the M_o value is low, but of course the arch has twisted and the resultant of both in-plane & out-of-plane moments is 596 kNm. Even for the extreme case of $\theta = \pi/64$ (span/rise=80) the deflection with this model is predicted as 0.595m (close to the straight beam value of $PL^3/384EI = 0.592$m). The model is clearly very inaccurate at the lowest span/rise ratio of 2 (semi-circle), but at more realistic span/rise ratios at or above 5 it becomes acceptable. The results in table 1 for the torsion/bending model appear generally good, but the transverse deformations of the shallowest arch beams are greatly in error – due to the restricted value of torsion factor required to obtain convergence. Overall, the end shears model appears to be the only suitable one for very shallow arches.

The results in table 1 for the torsion/bending model appear generally good, but the transverse deformations of the shallowest arch beams are greatly in error – due to the restricted value of the torsion factor required to obtain convergence. Overall the end shears model appears to be the only suitable one for very shallow arches.

For arches of compound shape comprising differing radii, and/or spatially curved arches, the two systems can be combined – with "splines" (using end shears) coupled by torsion/bending "splices" with five segments.

5 ANALYSIS OF A COUPLED MEMBRANE/ARCH SYSTEM

The following studies are for a symmetric membrane structure of about 3100m^2 supported by a central arch of 100m span and 16m rise. The arch has the same properties previously

used for the studies in table 1: with EA = 5400 kN, EI = 220 MNm^2 and slenderness ratio of about 530; for all of the studies the arch is sub-divided into 48 segments. The form of the structure is shown in the attached plot files **arcz0** (plan view), **arcx0** (view in direction x) and arcy0 (view in direction y) – note that x and y plots have different scales. The latter elevations are rotated by 1° about the y and x axes respectively, and all subsequent elevation plots for the various loaded states are similarly denoted and presented. The membrane is divided into two main regions with four "panels" per region, each containing one edge scallop. Asymmetric loading is applied as uniform snow loading p on panels 1 & 2 of region 1 only. Thus quarter of the structure is loaded, and the loading induces sway of the arch in both the x and y directions.

For the torsion/bending model the initial geometry and properties of the arch suggest an appropriate torsion factor T_{fac}= 0.35 (using equation 16 with 14b & 15b and C1= 1). However, as the arch deforms under high loadings the value of T_{fac} should be reduced (ultimately to a very low value, but restricted by conditions for numerical convergence). For the studies below the lowest value of T_{fac} which could be used was approximately 0.035; some results in table 2 for torsion/bending models are therefore given for both these values of T_{fac}.

In table 2, the notation used for the various models and results is **arcT1** for the torsion/bending model with p=1 kN/m^2 and T_{fac} = 0.35, **arcT1c** for the same loading, but T_{fac} = 0.035, and **arcS1** for the same loading using end shears model. Similar notations are used for the alternative loading intensities as listed in the table. Models for which deformed state plots are attached are denoted * (the notation for these plots being **arcSx1 & arcSy1** for model **arcS1** * etc.). The values tabulated in table 2 for each test model and loading are $\delta 1$ = the transverse (or y) deflection at the ¼ point of the arch between panels 1 & 2, C_{max} = maximum compression in the arch, M_{o1} & M_{o2} – the out-of-plane (or transverse) moments at the two ¼ points of the arch, M_{i1} & M_{i2} the in-plane moments at the ¼ points, and for the torsion/bending models T = maximum torsion (at crown point).

In addition to the plots indicated in the table for the various stable load states (up to 1.35 kN/m^2), plots **arcSx4** and **arcSy4** are included which show, for the end shears model, the initial stages of snap-through buckling; this occurred at a load level of p = 1.42 kN/m^2.

Table 4: Bending and twisting moment results for a series of coupled arch/membrane systems

Model	p kN/m2	T_{fac}	δ_1	Cmax kN	M_{o1}	M_{o2}	M_{i1}	M_{i2}	T
arcT1	1	0.35	0.737	1564	-1729	886	-1099	1064	382
arcT1c *	1	0.035	0.898	1640	-1051	445	-1051	1171	106
arcS1 *	1	-	0.897	1627	-684	709	-1120	1161	-
arcT01	0.1	0.35	0.0728	615	-161	104	-74	107	37
arcS01	0.1	-	0.0806	617	-78	45	-77	109	-
arcT3c	1.35	0.035	1.476	2209	-1592	634	-1850	1996	169
arcS3 *	1.35	-	1.447	2174	-993	1403	-1568	1931	-

5 DISCUSSION OF RESULTS

For the load level p = 1.0 kN/m^2 the results for transverse deflection, maximum arch compression, and the in-plane moments at ¼ points are similar for each model, but for the torsion/bending model the maximum predicted out-of-plane moment is much greater, particularly for the stiffer arch with T_{fac} = 0.35. As T_{fac} reduces the results become closer, and the lower value of T_{fac} is probably more realistic since the arch has become very flat in the loaded area (view arcTy1). The results show a similar pattern to the first set of tests: deflections, compressions, and in-plane moments are in reasonable agreement for all models, but the transverse moments predicted by the torsion/bending model are significantly different to those of the end shears model.

A much more significant issue is the collapse load modelling of flexible arch structures. The torsion/bending model cannot actually achieve snap-through since when it flattens it becomes quasi-stable (neither diverging nor converging but oscillating between two states). The nearest approach was a loading intensity of 1.35 kN/m^2 as given in table 2, and in order to obtain those results a gradual approach was necessary, using successively reducing values of T_{fac} and increasing fictitious masses (or conditioning factor); in all, four stages were used, each with many thousands of iterations. In contrast the end shears model converged fully at least 10 x faster. At this higher loading (near collapse) the results for deflections, compressions and in-plane moments are very similar for all models, but the transverse moments predicted by the torsion/bending model are again much higher. However, it is demonstrated in the following that the end shears model does give the correct solution for the ultimate snap-through collapse.

In the analysis of the torsion/bending model the in-plane moments at all interior nodes are computed at each iteration as M_i = EI x ($\mathbf{1/R - 1/R_0}$) where $\mathbf{1/R}$ is the current curvature and $\mathbf{1/R_0}$ is the initial curvature in the unstrained state. For the end shears model that expression is used only for the moment applied to set the correcting/fictitious shears in the end links (S = M_i /L). For all other (interior) links of the arch the shears are set as S = (M_i + M_j)/L where the moments at the link nodes i or j are set using only the current curvature: M_i = EI x ($\mathbf{1/R}$) since the initial curvature effects are internally cancelled. (At the output stage of course these

moments are determined using the change of curvature from the initial state). It has been noted previously in section 1 (equations 6) that the initial in-plane curvature of a spline bent from straight (as in the end shears model) provides substantial geometric stiffness to out-of–plane movements, but for a section of an arch which has flattened and lost all of this curvature, the bending resistance to movements in both the radial and transverse directions is the same value based on the subsequent curvature departure from this straight state.

To provide a check on the validity of the failure load prediction of 1.42 kN/m^2 by the end shears model, and the extent to which this solution may be path dependent, the following sequence of loadings were run using the end shears model: Half symmetric loading of 0.8 kN/m^2 on panels 1 and 2 of both regions 1 and 2 – this produced deformations which had practically flattened the loaded area of the arch (with no out-of-plane deformations). Using the above deformed state as a starting condition the loads were redistributed to 1.0 kN/m^2 on panels 1 & 2 of region 1 and 0.5 kN/m^2 on panels 1 & 2 of region 2. From this second state, all of the loading in region 2 was then released and the loading in region 1 increased to 1.4 kN/m^2 on panels 1 & 2. As a check on the deflections and stress resultants predicted from this run the structure was re-run with this loading applied to the zero condition (prestress state); the results obtained were identical. On the basis of these studies it is reasonable to conclude that the snap-through failure loading of 1.42 kN/m^2 predicted by the end shears model is reliable.

8 PLOTS OF THE INITIAL AND DEFORMED STATES OF THE ARCH SUPPORTED MEMBRANE

8.1 Initial prestress form of the structure

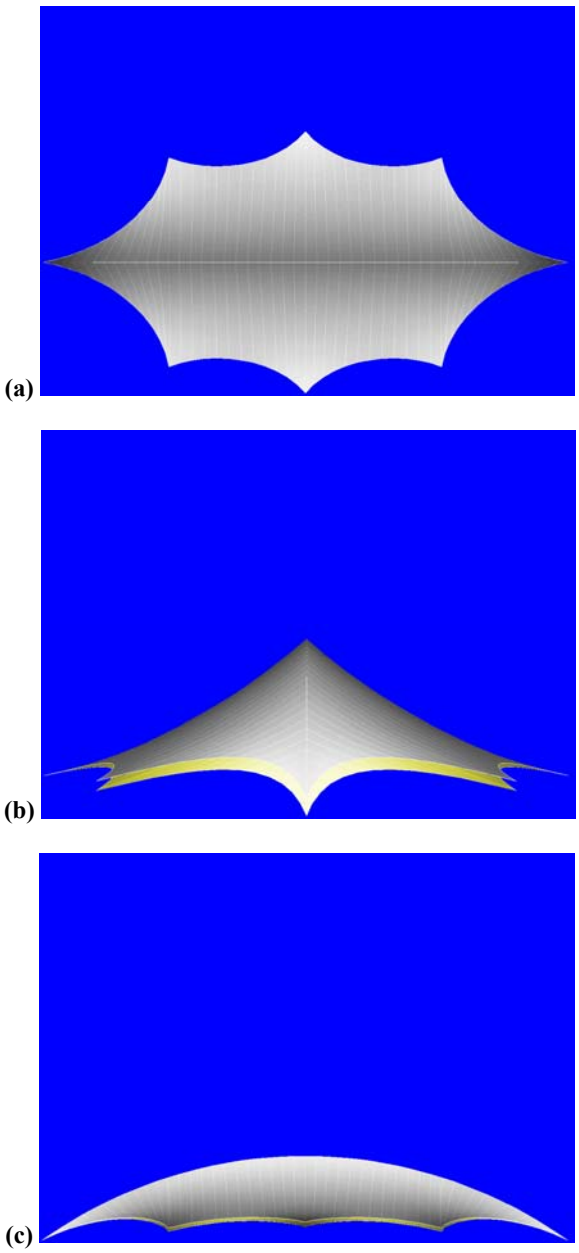

Figure 20: (a) Plan View arcz0, (b)arcx0, (c)arcy0

8.2 Deformed states

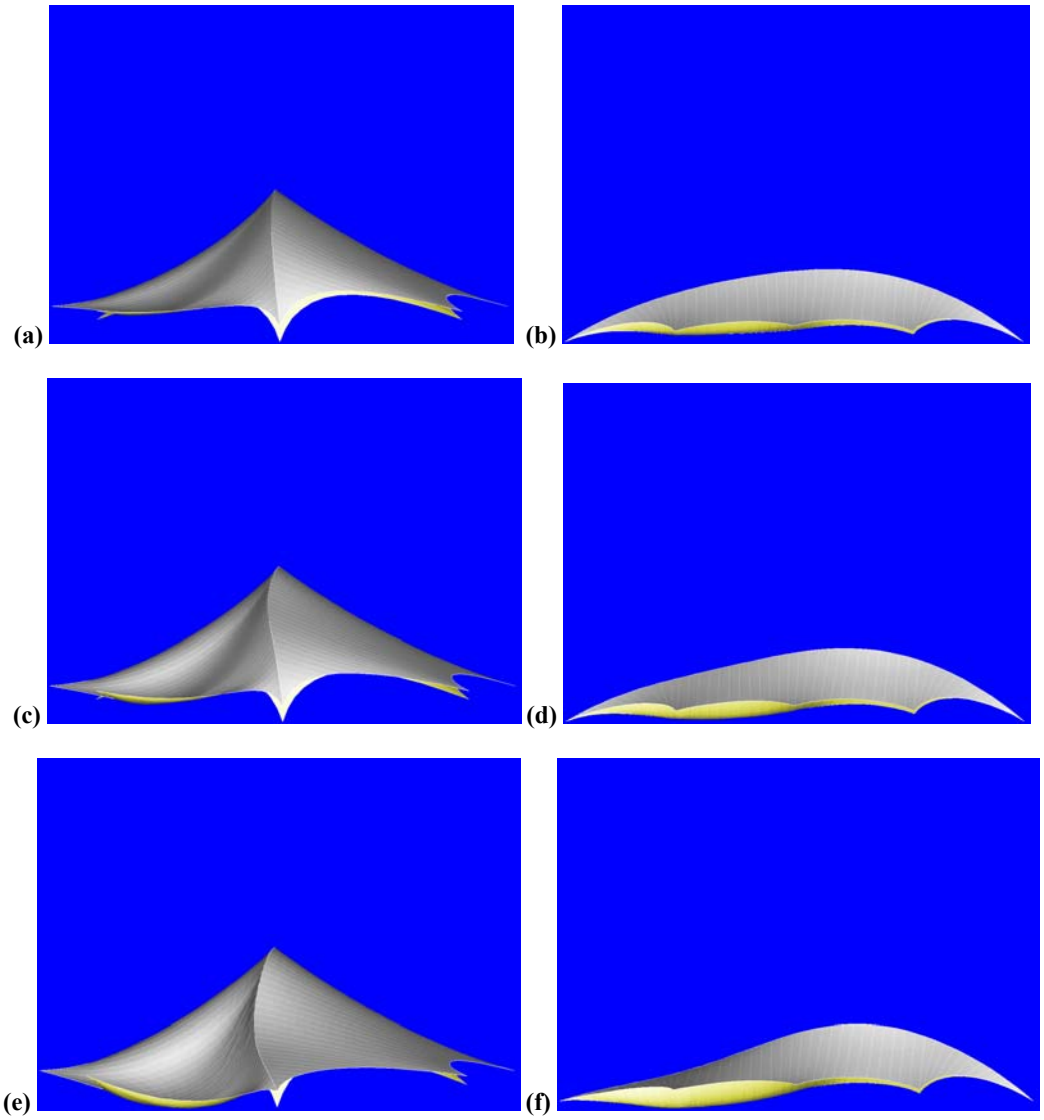

Figure 31: (a) arcSx1, (b) arcSy1, (c) arcSx3, (d) arcSy3, (e) arcSx4, (f) arcSy4

REFERENCES

[1] Barnes M. R., Form finding and analysis of tension structures by dynamic relaxation, Int. Journal of Space Structures, v 14, n2, 1999, 89 – 104

[2] Barnes M. R., Adriaenssens S., Enclosed network bridges for urban environments, Int. Conf. on Adaptation and Movement in Architecture, Toronto, Canada, Oct 2013

[3] Barnes M. R., Adriaenssens S., Krupka M., A novel torsion/bending element for dynamic relaxation, Computers and Structures, 119, 2013, 60 - 67